SMART-1

AMIE

*A*dvanced *M*oon micro-*I*mager *E*xperiment

Estimation of the AMIE focal plane temperature at image acquisition times

Document number	S1-AMIE-SGS-TN-012
Issue/Revision	1/-
Date	2008-Jan-04

Prepared by	Björn Grieger	ESA/SCI-OS
	Miguel Almeida	ESA/SCI-OS
	Virgile Dougnac	microcameras
	Detlef Koschny	ESA/SCI-OS
	Santa Martinez	ESA/SCI-OS

Document change record			
Iss./Rev.	Date	Sections affected	Description
D/-	2007-Dec-07		Draft completed.
1/-	2008-Jan-04	1.3	Added remark on images without exposure times.

Contents

1 General items

1.1 Scope

The SMART-1 SC contains a number of scientific instruments, a few of them being remote sensing instruments. One of them is AMIE, a camera with 5.4° FOV and a total of 8 fixed filters in front of its CCD detector. The dark correction of the AMIE images requires to know the CCD temperature at the time of image acquisition. Herein, we describe how this temperature can be estimated from the available temperature measurements.

1.2 Introduction

The AMIE focal plane temperature is measured by a sensor in AMIE unit 1 [S1-AMI-MA-3001]. The sensor is read out if a respective telecommand is issued, what was usually done at the beginning of an imaging sequence. In this

nominal case, the simplest way to obtain a reasonable estimation of the focal plane temperature at the acquisition time of an image is obviously just to take the most recent temperature read out. However, the situation can be more complicated. A method to estimate the temperature at image acquisition time by an optimally weighted average of close in time measurements is described in section 2.

There are cases where no AMIE unit 1 temperature sensor readings have been taken for a longer time period. We have 9725 images with no temperature measurement within one hour before or after image acquisition. However, another sensor at the TRP was monitored by the SC almost continuously with a time step of the order of one minute. A method to model the AMIE focal plane temperature based on the TRP temperature taking into account the heat production by the AMIE instrument is described in section 3.

While our main objective of using the TRP data was to provide temperatures where no AMIE unit 1 measurements are available, the method can provide a second temperature estimation where a first one is already available from the AMIE measurements. In section 4 we describe how these two values are combined to the most accurate estimation.

1.3 Brief summary of results

The following tables show the number of images for which we obtained temperature estimations by different methods and the respective errors. Please note that herein we consider only images for which exposure times are available. These are almost all images, however, there are a few images without exposure times, 14 in the Earth Escape Phase and 2 in the Extended Mission Phase. Therefore our counts of total images differ respectively from the total number of images present in the data sets.

We present one table comprising the complete mission and one table for each of the three mission phases separately. The six rows of each table have the following meaning:

1. The simle method of just taking the last AMIE unit 1 temperature sensor reading as temperature at image acquision time. The number of images is the number for which this measurement was not longer than five minutes before image acquisition. An error is not estimated.

2. The Kriging method described in detail in section 2. It is applied to images where there is at least one unit 1 temperature measurement within one hour before or after image acquisition. For each image, an individual error of the temperature estimation is computed. The minimum, mean, and maximum error of all temprature estimations is given.

3. Modelling the AMIE focal plane temperature based on the SC TRP measurements and heat production by the active instrument, as described in detail in section 3. It is only applied to an image if the acquisition time does not fall in a gap beteen two successive TRP measurements larger than two hours. A global error of the model is given.

4. The RMS difference between the kriging result and the modelling result for images where both results are available. This value is discussed in section 4.1.

5. Combining the kriging and the modelling results if at least one of them is available as described in section 4. If both results are availabe for an image, an optimum weighted average is computed. The error of the combination is always smaller than the error or each individual result. The mean error of all combinations can be larger than the mean error of the kriging results if there are images for which only the modelling result is available.

6. Just the total number of images for comparison.

At the end we are left with with only 70 images for which we can not provide a temperature estimation. For all other 36372 images, we have a temperature with an error not larger than 1.24 K, with the error being on average 0.78 K.

1.3.1 All Phases

Ref	Method	Images	Min σ	Mean σ	Max σ
1	Simple	23210			
2	Kriging	26717	0.73	0.88	2.58
3	Modelling	32815		1.24	
4	RMS diff	23160		0.95	
5	Combined	36372	0.63	0.78	1.24
6	Total	36442			

1.3.2 Earth Escape Phase

Ref	Method	Images	Min σ	Mean σ	Max σ
1	Simple	4498			
2	Kriging	4498	0.73	0.78	1.00
3	Modelling	3590		1.24	
4	RMS diff	3589		1.31	
5	Combined	4499	0.63	0.68	1.24
6	Total	4499			

1.3.3 Lunar Phase

Ref	Method	Images	Min σ	Mean σ	Max σ
1	Simple	9257			
2	Kriging	12433	0.73	0.92	2.35
3	Modelling	10526		1.24	
4	RMS diff	9923		0.68	
5	Combined	13036	0.63	0.77	1.24
6	Total	13036			

1.3.4 Extended Mission

Ref	Method	Images	Min σ	Mean σ	Max σ
1	Simple	9455			
2	Kriging	9786	0.73	0.88	2.58
3	Modelling	18699		1.24	
5	RMS diff	9648		1.02	
4	Combined	18837	0.63	0.99	1.24
6	Total	18907			

1.4 Reference documents

[Armstrong-1998] Margatet Armstrong, Basic Linear Geostatistics, Springer, 1998.

[S1-AMI-MA-3001] Flight User Manual (Iss./Rev. 2.1, 2003-Jan-30)

1.5 Abbreviations

AMIE	Advanced Moon Imaging Experiment
CCD	Charge Coupled Device
FOV	Field Of View
RMS	Root Mean Square
SC	Spacecraft
SMART	Small Missions for Advanced Research in Technology
TRP	Temperature Reference Point

2 Estimation from AMIE unit 1 temperature data

2.1 Description of the problem

There are 25254 temperature readings from the sensor in AMIE unit 1, which cover the time range from 2003-10-03 to 2006-09-03. During this time, the AMIE camera took 36442 images (counting only those which were successfully downloaded and unpacked). Image acquisition and temperature sensor reading did not occur at the same time. The simplest way to obtain an estimation for the focal plane temperature at image acquisition time would be to just take the value of the closest-in-time temperature measurement. However, we can easily identify situations where a more comprehensive approach is desirable:

- If there is more than one temperature measurement close in time, it would be advantages to average all close measurements to reduce the error of the individual measurement.
- If the closest temperature measurements occurred a considerable time before and after image acquisition, the temperature should be reasonably interpolated.

Thus, the estimation of the temperature at image acquisition time should be a weighted average of all close-in-time temperature measurements. The method

to obtain the optimum weights for such an averaging is called kriging after its inventor Daniel Krige. It is described in the next section.

2.2 Overview of the kriging approach

Kriging is a method to estimate the value of a quantity at a location (or, in our case, a at time) where no measurement is available from available nearby measurements. The kriging solution is fully determined by the following constraints:

- The estimation is a weighted sum of the measurements.
- The estimation is unbiased, i. e., the expectation value of the estimation equals the expectation value of the measurement.
- The weights are chosen so that the variance (i.e., the error) of the estimation is minimized.

Thus, kriging provides the optimum weights for the estimation by a weighted sum.

The method of kriging involves two main steps:

1. From all the measurements, the so-called *variogram* is estimated, which describes the spatial (or, in our case, the temporal) correlation of the data.
2. The variogram provides the coefficients for a linear equation system, the so-called kriging system, the solution of which gives the optimum weights for the weighted sum of measurements.

The application of these two steps to the AMIE unit 1 temperature data is described in sections 2.3 and 2.4, respectively.

2.3 The variogram of the AMIE unit 1 temperature measurements

The variogram is defined as

$$\gamma(\Delta t) = \frac{1}{2} \left\langle (T(t + \Delta t) - T(t))^2 \right\rangle , \tag{1}$$

where Δt is the time difference between two temperature measurements, $T(t)$ is the temperature measured at time t, and $\langle \ldots \rangle$ denotes the expectation value. The variogram $\gamma(\Delta t)$ can be estimated by looping through all *pairs* of available measurements and summing up their squared differences in appropriate bins. The result for the AMIE unit 1 temperature measurements is shown in Fig. 1.

As stated in section 2.2, the variogram is used to set up a system of linear equations, the kriging system. To obtain a well posed equation system, the variogram has to fulfill certain conditions. In general, the variogram computed numerically from the data, the so-called experimental variogram, does not fulfill these conditions. Therefore it is common practice to fit a variogram model to

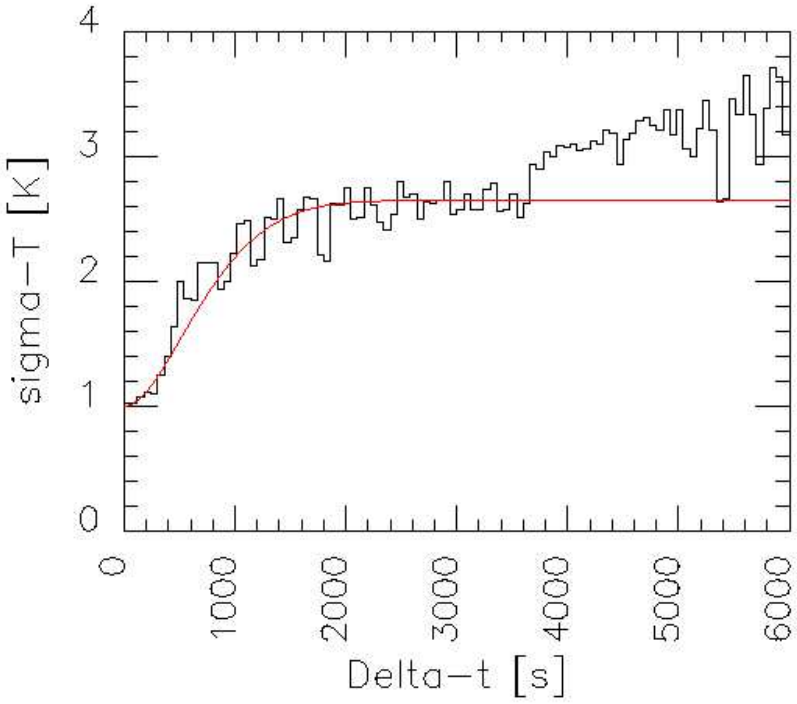

Figure 1: Variogram of the AMIE unit 1 temperature data. Instead of $\gamma(\Delta t)$ directly, we have plotted $\sqrt{2\,\gamma(\Delta t)}$. In this way, the ordinate illustrates the expected difference in Kelvin for two measurements Δt apart. The experimental variogram is plotted black, the fitted variogram model is plotted in red.

the data. A variogram model is a parameterized function which is known to fulfill all conditions for a well formed variogram. Various variogram model functions are available. The function we have fitted in Fig. 1 is a Gaussian variogram model given by

$$\gamma(\Delta t) = \frac{1}{2}\left(6\,\mathrm{K}^2 \cdot \left(1 - \mathrm{e}^{-(\Delta t/1000\,\mathrm{s})^2}\right) + 1\,\mathrm{K}^2\right). \tag{2}$$

For $\Delta t \to 0$ we get $\sqrt{2\,\gamma(\Delta t)} = 1\,\mathrm{K}$. This is the expectation value for the difference of two measurements taken at almost the same time. In our case this reflects the measurement error of the temperature sensor. The standard deviation of an AMIE unit 1 mesurement from the true temperature value is

$$\sigma_1 = \sqrt{\gamma(\Delta t \to 0)} = 0.71\,\mathrm{K}. \tag{3}$$

We note that for $\Delta t > 3600\,\mathrm{s}$, the experimental variogram starts to deviate from the variogram model. Probably we are facing multiple nested variograms reflecting processes acting on different timescales, e. g., thermal fluxes acting on time scales shorter than one hour and influences of SC attitude changes typically acting on longer time scales. We will take this into account by only considering measurements that are not more than one hour away from an image acquisition time. We do not expect data beyond this time difference to be significant anyway. Moreover, we have to somehow limit the number of temperature data points which we use for an image, as the number of data points determines the rank of the equation system we have to solve. It would be impossible (with our computational resources) to use the total number of 25254 data points.

2.4 Solving the kriging system for the AMIE unit 1 temperature measurements

The kriging system has to be solved for each image acquisition time to obtain the weights to estimate the temperature at that time from close-in-time measurements. The equation system looks like this:

$$\begin{bmatrix} 0 & \gamma_{1,2} & \dots & \gamma_{1,N} & 1 \\ \gamma_{2,1} & 0 & \dots & \gamma_{2,N} & 1 \\ \vdots & \vdots & & \vdots & \vdots \\ \gamma_{N,1} & \gamma_{N,2} & \dots & 0 & 1 \\ 1 & 1 & \dots & 1 & 0 \end{bmatrix} \times \begin{bmatrix} \lambda_1 \\ \lambda_2 \\ \vdots \\ \lambda_N \\ \mu \end{bmatrix} = \begin{bmatrix} \gamma_{1,0} \\ \gamma_{2,0} \\ \vdots \\ \gamma_{N,0} \\ 1 \end{bmatrix} \tag{4}$$

Here is

$$\gamma_{i,j} = \gamma(|t_i - t_j|), \tag{5}$$

with $(t_i)_{i=1,N}$ being the times of the temperature measurements $(T_i)_{i=1,N}$ and t_0 being the image acquisition time in question. The values $(\lambda_i)_{i=1,N}$ which result from the solution of the equation system are just the weights for the estimation of the temperature T_{krig} at time t_0, i. e.,

$$T_{\mathrm{krig}} = \sum_{i=1}^{N} \lambda_i\, T_i. \tag{6}$$

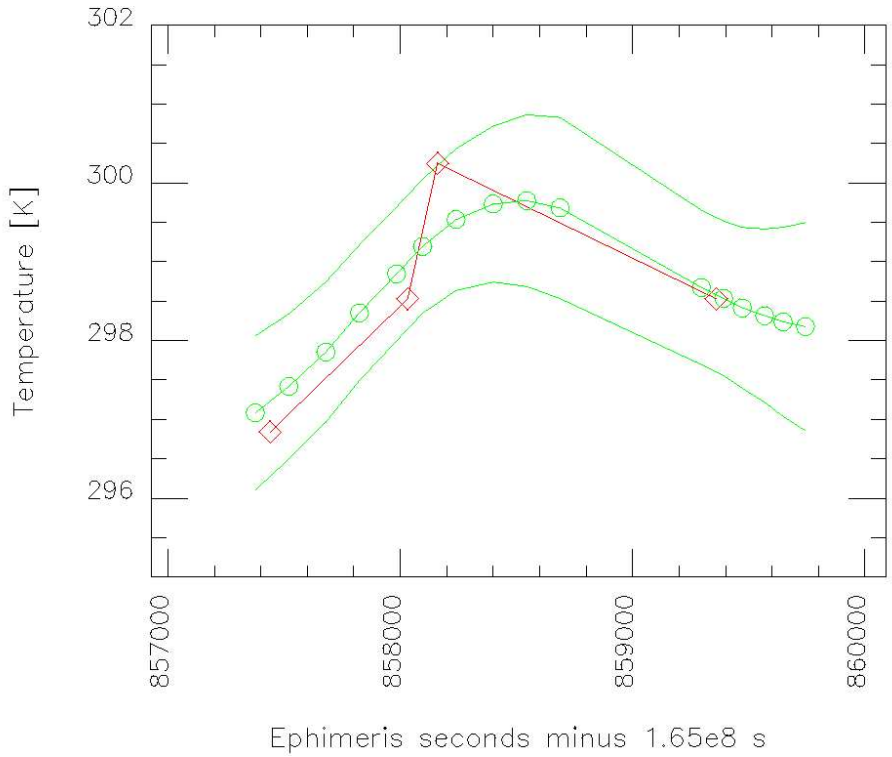

Figure 2: Example of kriging temperatures from the AMIE unit 1 measurements. The measurements are plotted in red. The kriging results are shown in green, with the circles marking the image acquisition times. The green lines without marks indicate the error of $\pm 1\sigma$.

From the resultant value for the Lagrange multiplier μ, we can obtain the variance of the estimated temperature:

$$\sigma^2_{\text{krig}} = \sum_{i=1}^{N} \lambda_i \, \gamma_{i,0} + \mu. \tag{7}$$

We have to solve such an equation system for each of the 36442 images. For each image, we consider all temperature measurements within one hour before or after images acquisition. The number of measurements within this time period ranges from zero (then we cannot estimate a temperature) over just a few up to a few hundred, yielding equation systems of these ranks. The complete computation for all images takes about 30 seconds with Fortran using the LAPACK algebra library. The results are summarized in section 1.3.

2.5 Some examples of kriging results

To illustrate the temperatures resultant from kriging, we show a few example. A time period of 40 minutes duration from the Lunar Phase is shown in Fig. 2. We selected this time window to illustrate the behavior of kriging in the case that we only have sparse measurements. There are four temperature measure-

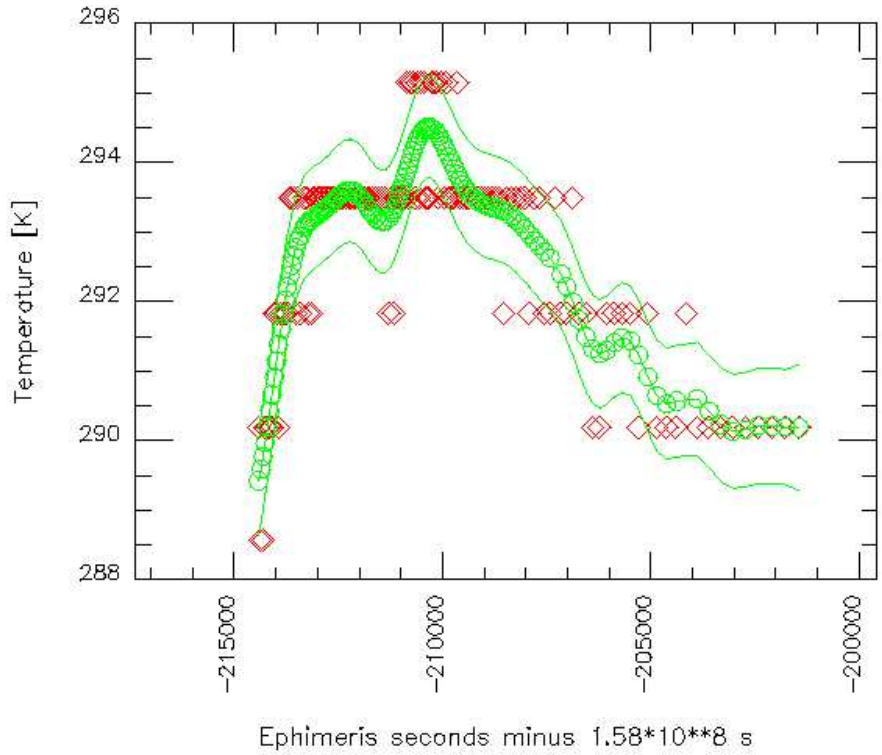

Figure 3: Example of kriging temperatures from the AMIE unit 1 measurements. The measurements are plotted in red. The kriging results are shown in green, with the circles marking the image acquisition times. The green lines without marks indicate the error of $\pm 1\sigma$.

ments. Note that the AMIE unit 1 sensor does only provide values in discrete steps of about 1.7 K.

We can notice that kriging does quite reasonably interpolate in between the data points. The leftmost kriged temperature is still slightly higher than the close by measurement because of the presence of the other measurements, which are also taken into account. The kriged values do not follow the spurious strong increase from the second to the third measurement, however, the uncertainty range does still encompass all data points. At the right hand margin, the uncertainty increases as we move away from the data points.

Another example, now of a case where we have a high density of temperature measurments, is shown in Fig. 3. It illustrates how kriging makes use of multiple near by measurements by averaging them in an optimum way.

3 Estimation from TRP data

3.1 Description of the problem

During the Extended Mission Phase (cf. section 1.3.4), we have more than 9121 images for which we cannot estimate a temperature in the way described in section 2.3, because the closest temperature measurement is more than one hour

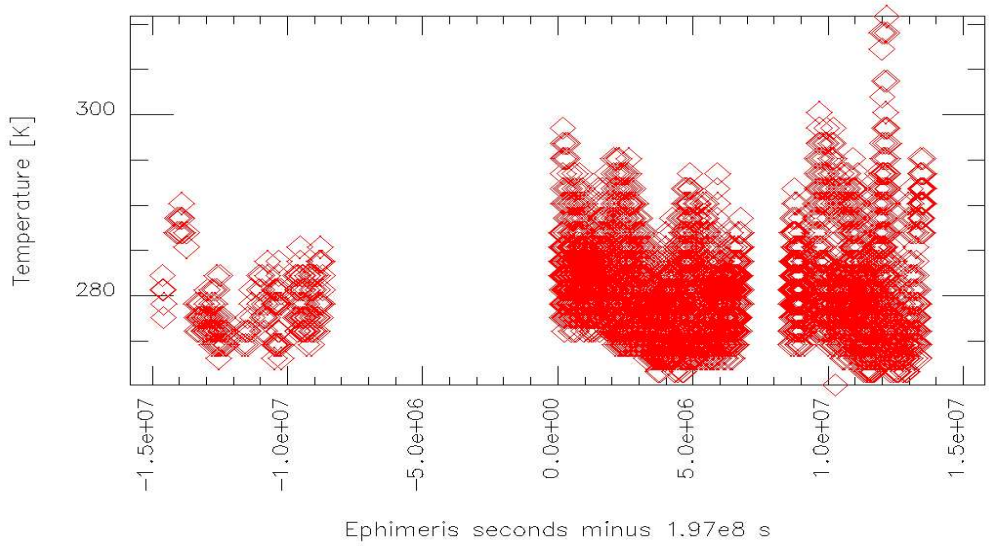

Figure 4: The temperature measurements taken with the AMIE unit 1 sensor during the Extended Mission Phase. The large gap ranges from 2005-12-19 to 2006-04-01.

away. Most of these "lonely images" stem from the time period between 2005-12-19 and 2006-04-01, where no temperature measurement at all was taken. This gap is illustrated in Fig. 4.

While we have this large gap and several smaller gaps in the AMIE unit 1 sensor readings, the temperature at the TRP was monitored by the SC almost continuously with a time step of the order of one minute. The TRP measurements during the Extended Mission Phase are shown in Fig. 5. Because of their good coverage, we may try to use the TRP measurements to estimate the AMIE focal plane temperature at image acquisition times. However, there is no straight forward correlation between AMIE unit 1 and TRP temperature. The cross-correlation function between these two is shown in Fig. 6. The highest correlation of 0.83 is obtained for AMIE unit 1 trailing the TRP by about 30 minutes. The value of 0.83 does not indicate a very high correlation. This can be illustrated by plotting pairs of TRP and AMIE unit 1 measurements which are separated by 25–35 minutes, see Fig. 7. We notice that knowledge of the TRP temperature does not constrain the AMIE unit 1 temperature very well. In fact, the RMS deviation between these two temperatures amounts to 3.12 K. Therefore, ussing the TRP data straight forward to estimate the AMIE focal plane temperature would not give very accurate results. In section 3.2 we shall investigate a more comprehensive approach which takes into account heating by the active AMIE instrument.

3.2 Modelling the AMIE focal plane temperature

If we closely inspect the time series of AMIE unit 1 and TRP temperature measurements, we notice a typical behaviour. One example of this can be seen just in the time period already presented in Fig. 3. The respective TRP data is

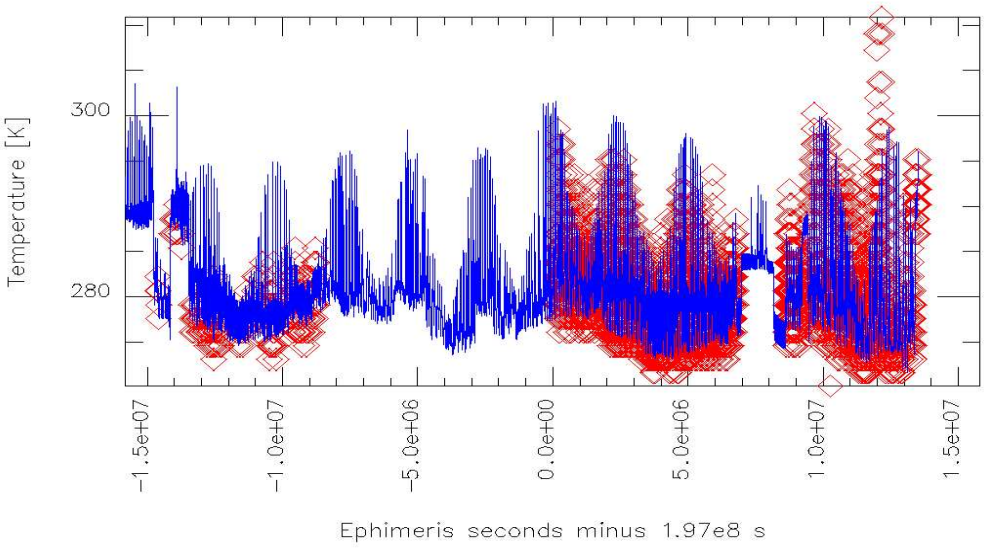

Figure 5: The temperature measurements taken with the sensor at the TRP (blue line), together with the AMIE unit 1 measurements (red diamonds) also shown in Fig. 4, during the Extended Mission Phase.

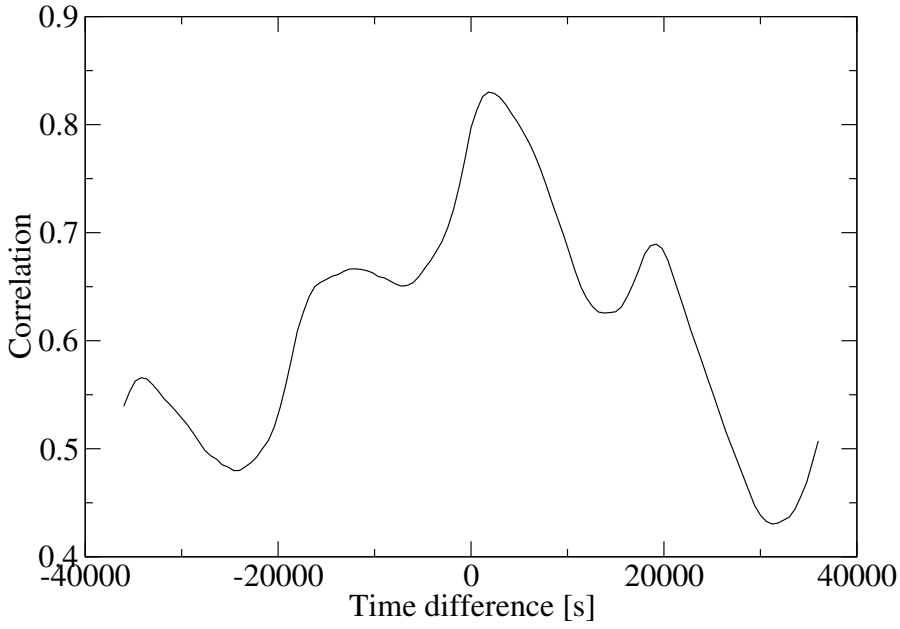

Figure 6: Cross-correlation function of AMIE unit 1 and TRP temperature measurements.

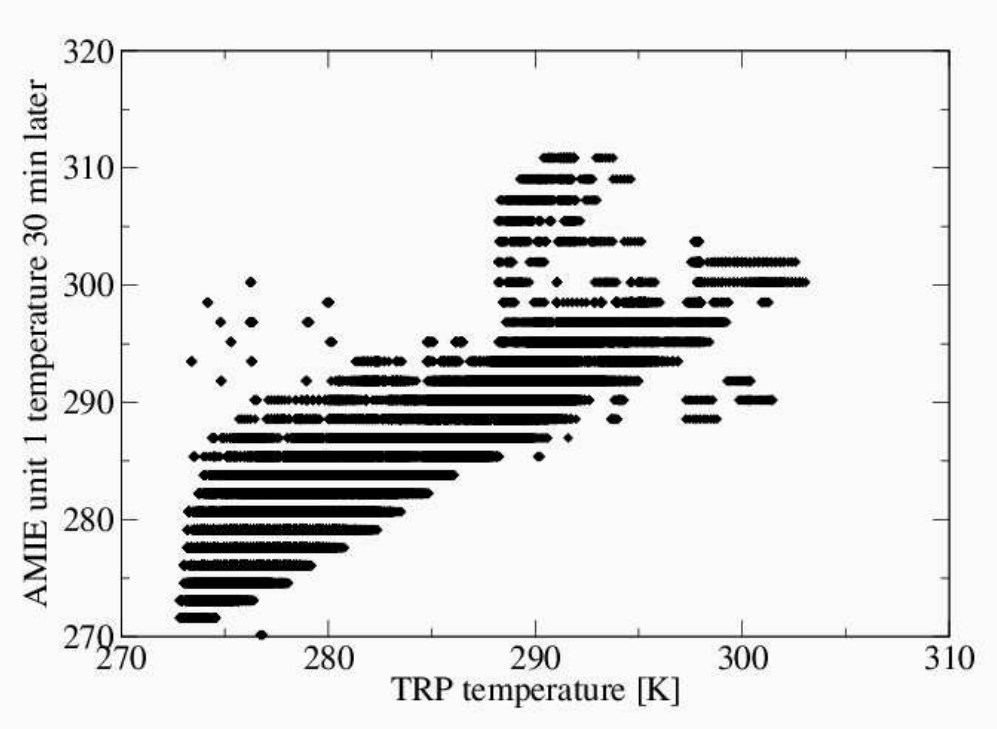

Figure 7: Pairs of TRP and AMIE unit 1 temperature measurements separated by 25–35 minutes. For this time difference, the highest correlation is expected.

shown together with the AMIE data in Fig. 8. After looking at many segments of the temperature time series like this one, we notice that excursions of the AMIE temperature from the TRP appear to be related to AMIE activity. If the camera is switched on, it obviously produces heat that increases the temperature with respect to the TRP. The heat production appears to be larger if images are taken with high frequency. These observations and various numerical experiments lead us to the following model for the AMIE focal plane temperature evolution:

$$\begin{aligned} T_{\mathrm{mod}}(t) &= T_{\mathrm{TRP}}(t) \\ &\quad + a \cdot (T_{\mathrm{AMIE}}(t - \Delta t) - T_{\mathrm{TRP}}(t)) \\ &\quad + F\,\Delta t \\ &\quad + T_{\mathrm{img}} \\ &\quad + \Delta T \end{aligned} \tag{8}$$

The quantities are in detail:

T_{TRP} is the TRP temperature. It is linearly interpolated between the closest previous and next measurements. If the gap between two successive measurements is larger than two hours, the TRP temperature is concidered to be inaccurate and the computed model temperature is not used subsequently.

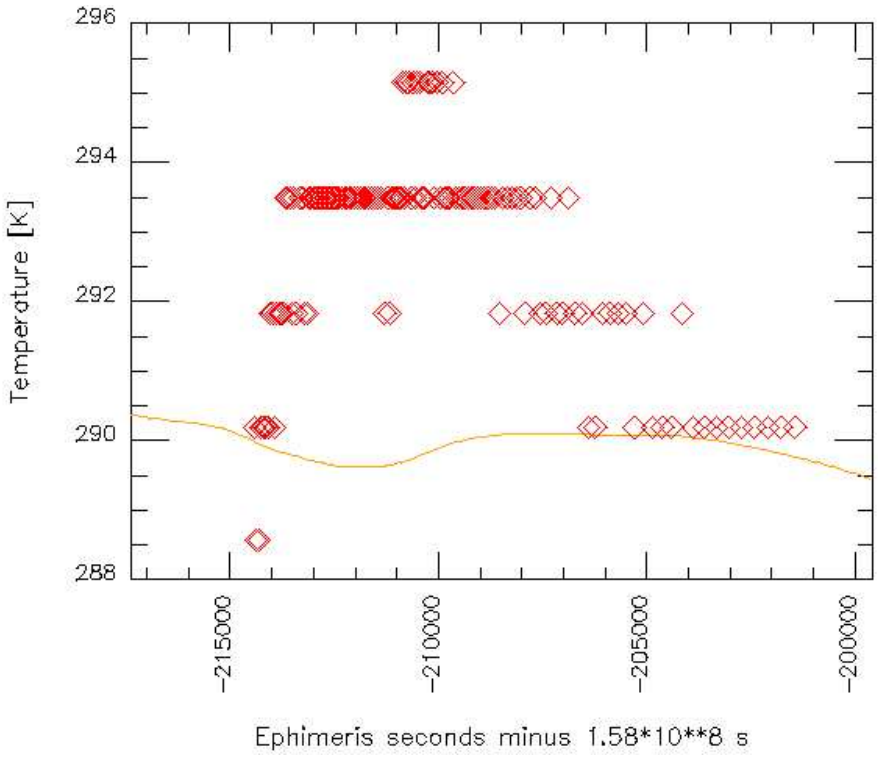

Figure 8: Temperatures measurements from the AMIE unit 1 sensor (red diamonds) together with measurements from the TRP sensor (orange line).

Δt is the time step. We use $\Delta t = 1\,\mathrm{s}$ to make sure that not more than one image is taken during a time step.

a is a damping factor describing exponential relaxation of the AMIE temperature towards the TRP temperature. For $\Delta t = 1$, the optimum value is $a = 0.99876$. This corresponds to an e-folding time of 13 minutes.

F describes the temperature increase due to heat production if the AMIE instrument is switched on. The optimum value is $F = 0.0243\,\mathrm{K/s}$. If AMIE is switched off, F is zero. The switch times are taken from the POR files.

T_{img} is the temperature increase due to taking one image. The optimum value is $T_{\mathrm{img}} = 0.0535\,\mathrm{K}$. If no image has been taken during Δt, then T_{img} is zero. The image acquisition times are taken from the POR files and not from the PDS labels of the images in the archive, because not all images which were taken have successfully been downloaded and unpacked.

ΔT is an offset between the AMIE unit 1 temperature sensor and the TRP sensor. The optimum value is $\Delta T = -0.613\,\mathrm{K}$.

The optimum values of the four model parameters have been found by minimizing the RMS error between the AMIE unit 1 temperature measurements and the respective model temperatures at the times of the measurements. AMIE

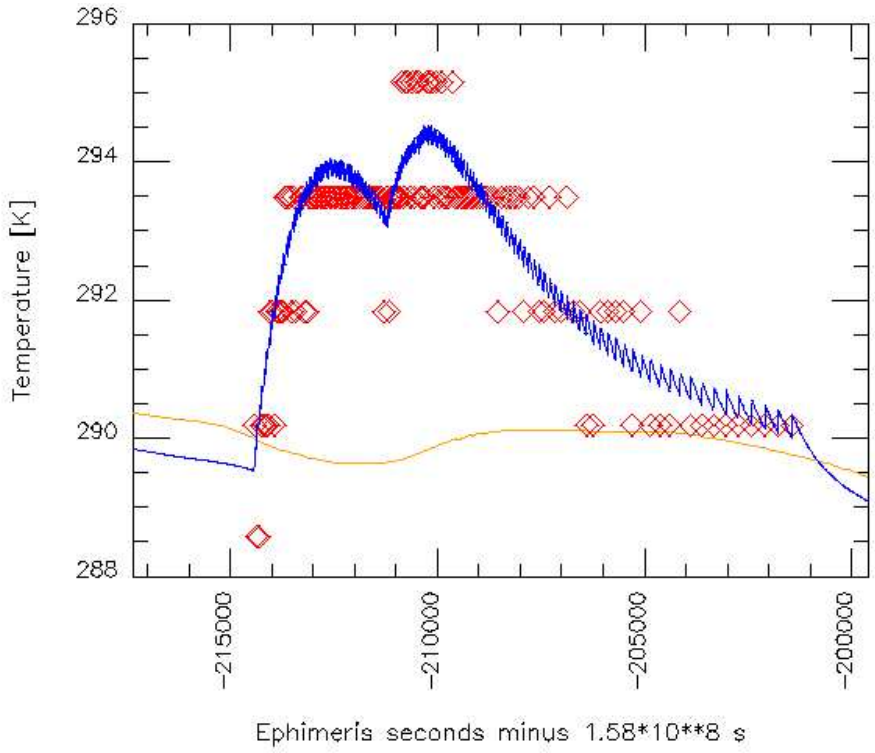

Figure 9: The modelled AMIE focal plane temperature (blue line) together with the measurements from the AMIE unit 1 sensor (red diamonds) and the measurements from the TRP sensor (orange line).

measurements which fall in a time gap larger than two hours between successive TRP measurements are not taken into acoount. Therefore only 21495 out of the totally availabel 25221 AMIE measurements have been used. Starting out from values grossly tuned by hand, the optimization is automatically performed by an evolutionary strategy, i. e., the parameter values are randomly changed from a starting point by small amounts until a smaller RMS deviation is achieved. Then the corresponding parameter set becomes the new starting point. The procedure is repeated until no better solution is found, which is the case after a few hundred iterations. The result is robust when starting from different initial values. The optimizatin takes about an hour of computation time.

The optimum model yields an RMS error between modeled and measured AMIE unit 1 temperatures of

$$\sigma_{\mathrm{mod}} = 1.24\,\mathrm{K}. \tag{9}$$

The consistency of this error estimation is investigated in section 4.1.

3.3 Some examples of modelling results

To illustrate the behaviour of the model, the result for the same time window as shown in Figs. 3 and 8 is presented in Fig. 9. The sawtooth features to the right are mainly due to repeated switching on and off of the intrument, while

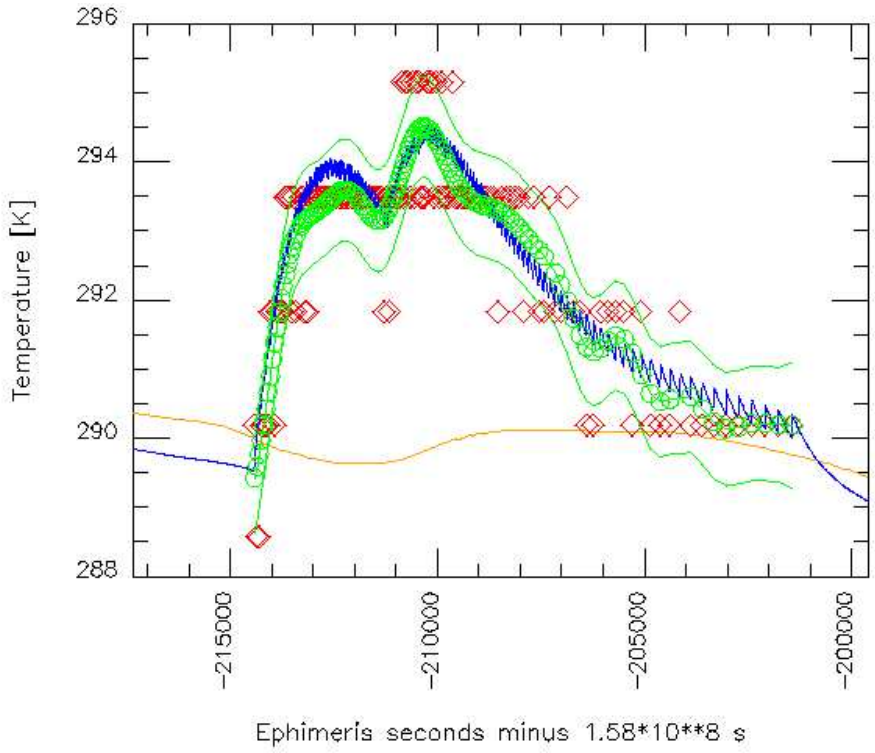

Figure 10: Comprison of the kriging results also shown in Fig. 3 (green) and the modelling results also shown in Fig. 9 (blue), together with the measurements from the AMIE unit 1 sensor (red diamonds) and the measurements from the TRP sensor (orange line).

rapid fluctuations slightly left of the center are also due to the heat produced by taking images at high frequency. The same model time series is compared with the kriging results in Fig. 10. The model results for the same time window as presented in Fig 2 are shown in Fig. 11. This example illustrates nicely the advantages and disadvantages of the two methods. At the left of the time window shown, we see that the kriging result deos not deviate conciderably from the measurement, while the model does. At the right we see that kriging can not reasonably extrapolate when no data is available, while the model can.

We should also show an example where the model does not fit quite well. In fact, this is the worst case we come across so far by visually browsing the results. It is shown in Fig. 12. One might think that the model could easily be tuned to fit here, but this would of course decrease the overall predictance skill of the optimized model.

The purpose of the modelling effort described in this section was to provide temperature estimations where no measurements of the AMIE unit 1 sensor are availabe. Thus we also show in Fig. 13 one modelling result for a time period almost centered in the large gap of temperature measurements in the Extended Mission Phase. In fact, this is a very typical example of an observation sequence during the large gap of AMIE temperature meassurements. There are many observation sequences which look quite similar. The temperature evolution

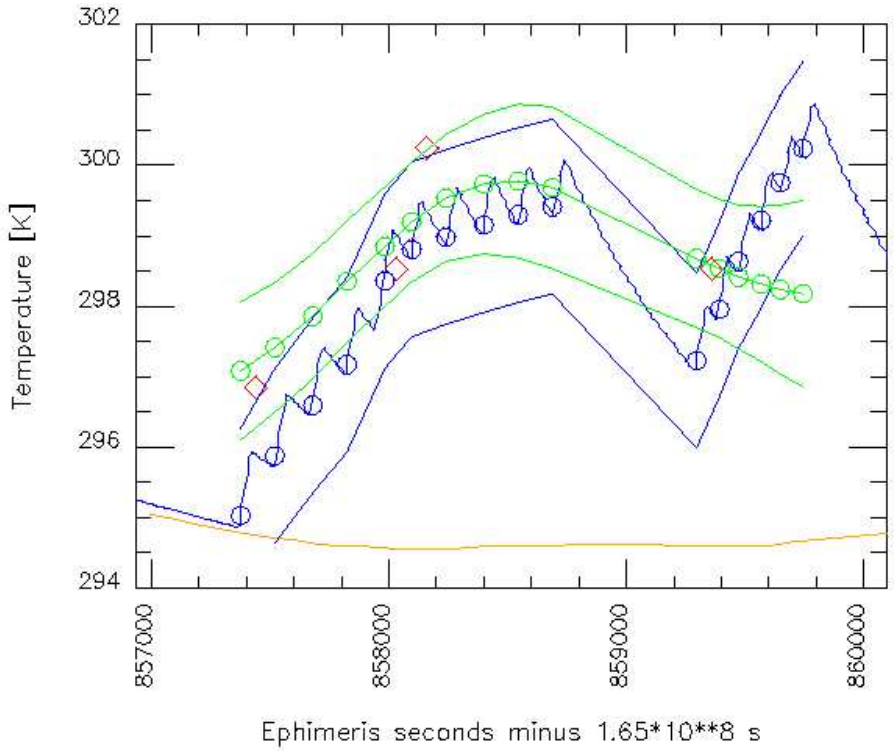

Figure 11: The kriging results also shown in Fig. 2 (green) and the modelling results (blue). Circles mark temperatures at image acquisition times. Green and blue lines without symbols indicate the error range. Also shown are the measurements from the AMIE unit 1 sensor (red diamonds) and the measurements from the TRP sensor (orange line).

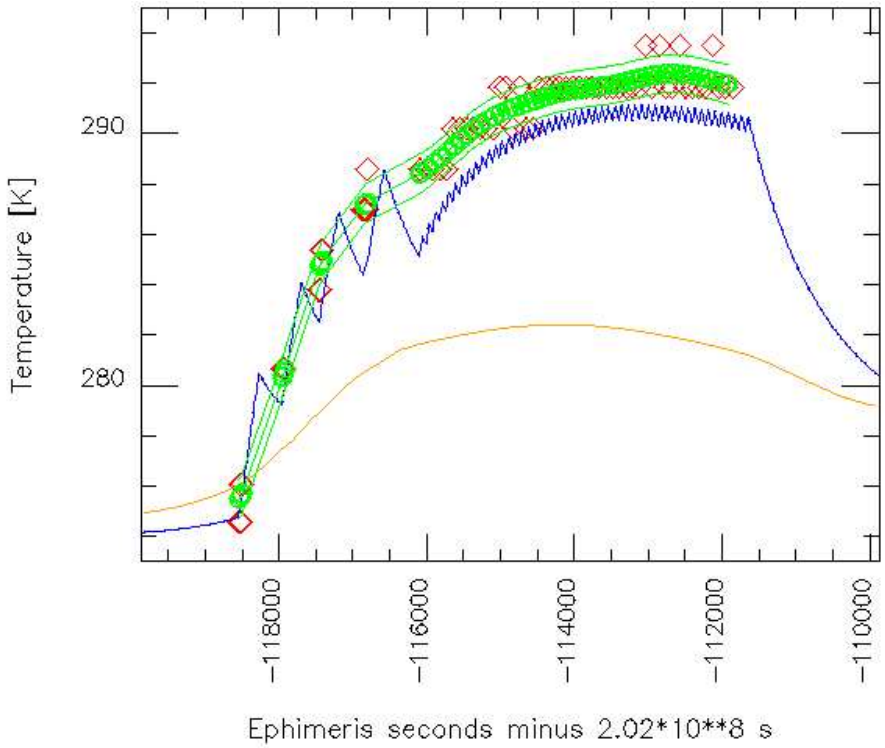

Figure 12: Kriging results (green) and modelling results (blue). Green circles mark kriged temperatures at image acquisition times. Green lines without symbols indicate the error range. Also shown are the measurements from the AMIE unit 1 sensor (red diamonds) and the measurements from the TRP sensor (orange line).

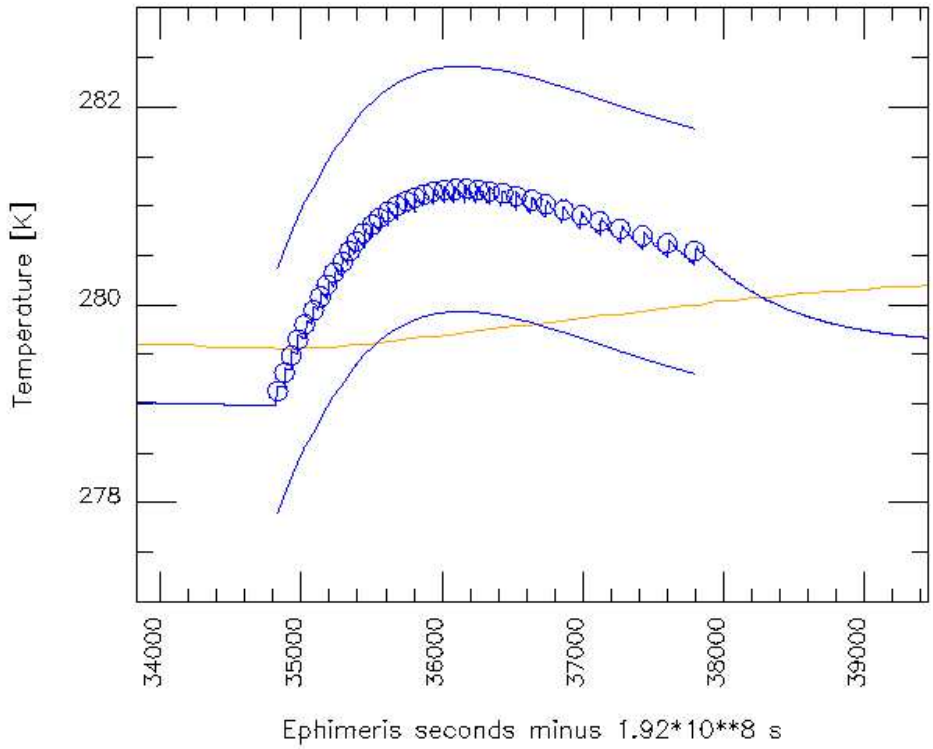

Figure 13: The modelled temperature for a time period in the large gap temperature measurements in the Extended Mission Phase. Circles mark temperatures at image acquisition times. The blue lines without symbols indicate the error range. Also shown are the measurements from the TRP sensor (orange line).

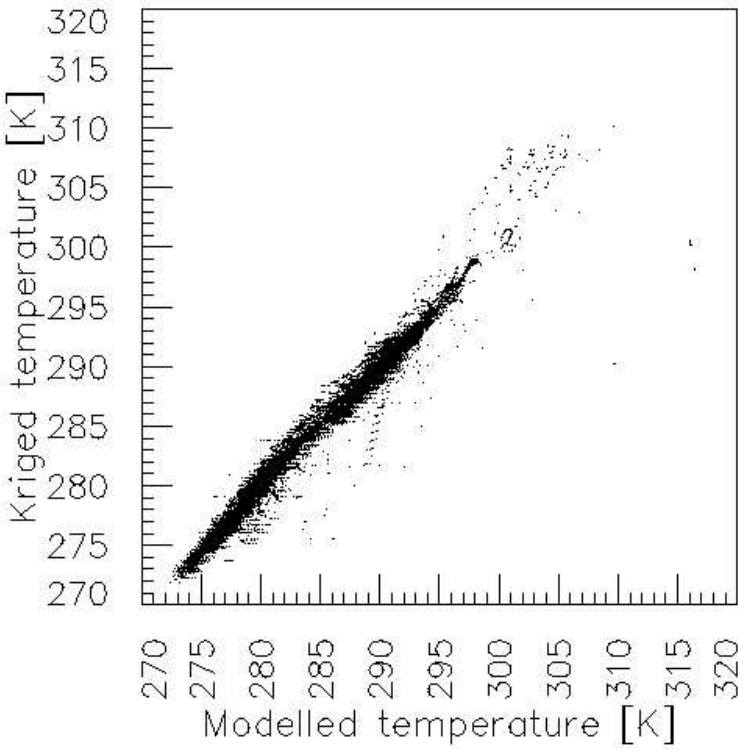

Figure 14: The correlation between temperature estimations by modelling (cf. section 3) and kriging (cf. section 2).

during such a sequence is relatively simple and the excursion from the TRP is not very large. Therefore we may have some confidence that our model is able to reasonably reproduce the AMIE focal plane temperature during this time period.

4 Combining temperature estimations from AMIE unit 1 and TRP

4.1 Consistency of error estimations

We have 23160 image acquisiton times for which we could compute the temperature with both methods, kriging of the AMIE measurements (section 2) and modelling based on the TRP measurements (section 3). The correlation between these two estimations is visualized in Fig. 14. We can also compute the RMS difference between these two temperature estimations. For all 23160 images, this difference amounts to

$$\sigma_{\text{diff}} = 0.95\,\text{K}, \tag{10}$$

cf. the table in section 1.3.1, or in terms of the variance:

$$\sigma^2_{\text{diff}} = 0.90\,\text{K}^2. \tag{11}$$

We would expect that this variance equals the sum of the variances of the two indivudual estimations, i. e.,

$$\sigma^2_{\mathrm{krig}} + \sigma^2_{\mathrm{mod}} = (0.88\,\mathrm{K})^2 + (1.24\,\mathrm{K})^2 = 2.31\,\mathrm{K}^2. \tag{12}$$

Obviously, the agreement between the results from the two methods is much better than expected from the individual variances. For the time being we can not offer an explanation for that.

4.2 Optimum weighted average of the two estimations

From the two temperature estimations T_{krig} and T_{mod} for a particular image and their respective errors σ_{krig} and σ_{mod}, we obtain the optimum combined estimation as

$$T_{\mathrm{comb}} = \frac{\frac{T_{\mathrm{krig}}}{\sigma^2_{\mathrm{krig}}} + \frac{T_{\mathrm{mod}}}{\sigma^2_{\mathrm{mod}}}}{\frac{1}{\sigma^2_{\mathrm{krig}}} + \frac{1}{\sigma^2_{\mathrm{mod}}}}. \tag{13}$$

4.3 The error of the combined temperature estimation

From the laws of error propagation, we obtain the variance of the combined temperature as

$$\sigma^2_{\mathrm{comb}} = \frac{1}{\frac{1}{\sigma^2_{\mathrm{krig}}} + \frac{1}{\sigma^2_{\mathrm{mod}}}}. \tag{14}$$

This value is always smaller than the minimum of σ^2_{krig} and σ^2_{mod}. If one of the variances is very large, σ^2_{comb} is close the the smaller one.

Eq. (14) does not take into account the variance of the actual sample, i. e., the difference between T_{krig} and T_{mod}. It can be shown that taking into account the sample variance leads to

$$\sigma'^2_{\mathrm{comb}} = \frac{1}{\frac{1}{\sigma^2_{\mathrm{krig}}} + \frac{1}{\sigma^2_{\mathrm{mod}}}} \cdot \frac{1}{n-1} \cdot \left(\frac{(T_{\mathrm{krig}} - T_{\mathrm{comb}})^2}{\sigma^2_{\mathrm{krig}}} + \frac{(T_{\mathrm{mod}} - T_{\mathrm{comb}})^2}{\sigma^2_{\mathrm{mod}}} \right), \tag{15}$$

where the number of samples is $n = 2$ in our case. However, because of the small sample, it is not reasonable to take its variance into account. Therefore we compute the standard deviations of the combined temperature estimations simply according to Eq. (14). The results are summarized in section 1.3. An example of combined temperature estimations and the respective errors for a previously shown time window is presented in Fig. 15.

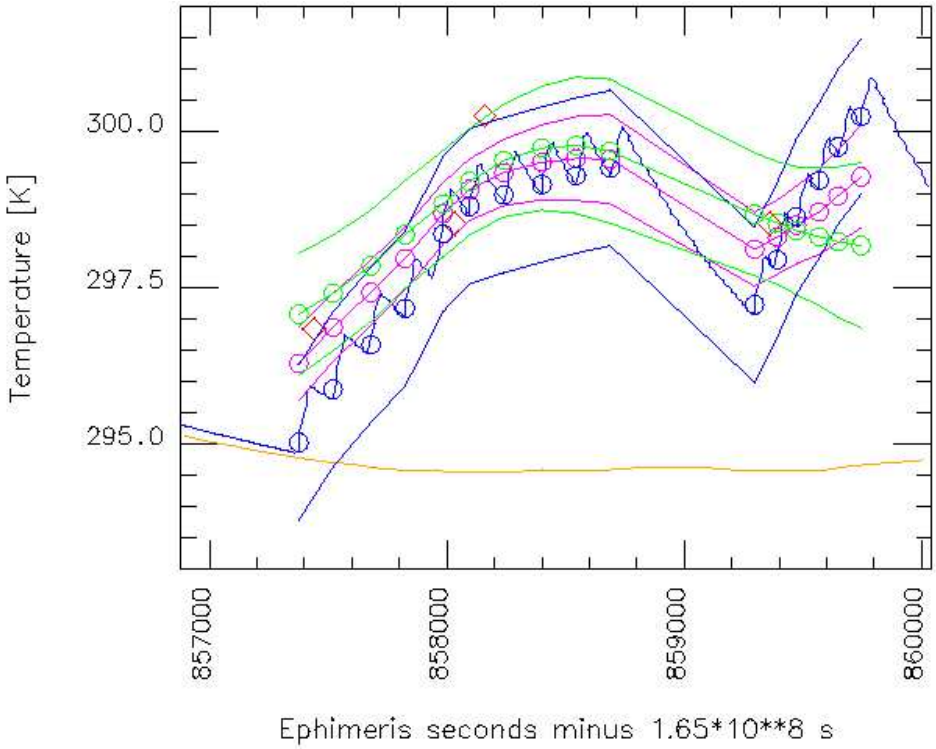

Figure 15: All temperature estimations together: Kriging results (green), modelling results (blue), and the combined value (magenta). Circles mark temperatures at image acquisition times. Lines without symbols indicate the error range. Also shown are the measurements from the AMIE unit 1 sensor (red diamonds) and the measurements from the TRP sensor (orange line).